HHS Public Access

Author manuscript

Nature. Author manuscript; available in PMC 2024 April 18.

Published in final edited form as:

Nature. 2024 February ; 626(8001): 1102–1107. doi:10.1038/s41586-024-07047-2.

Bone marrow plasma cells require P2rX4 to sense extracellular ATP

Masaki Ishikawa[1,2,‡], **Zainul S. Hasanali**[3], **Yongge Zhao**[1], **Arundhoti Das**[1], **Marieke Lavaert**[1], **Carly J. Roman**, **Jennifer Londregan**, **David Allman**[,‡], **Avinash Bhandoola**[1,‡]

[1]Laboratory of Genome Integrity, Center for Cancer Research, National Cancer Institute, National Institutes of Health, Bethesda, MD, 20892-4254, USA.

[2]Department of Pathology and Laboratory Medicine, Perelman School of Medicine at the University of Pennsylvania, Philadelphia, PA, 19104-6082, USA.

[3]Department of Medicine, Division of Hematology Oncology, Abramson Cancer Center at the University of Pennsylvania, Philadelphia, PA, 19104-5127, USA.

Abstract

Antibody-secreting plasma cells (PCs) produce antibodies and so play essential roles in immune protection[1]. PCs, including a long-lived subset, reside in the BM where they depend on poorly defined microenvironment-linked survival signals. We show that BM PCs use the ligand-gated purinergic ion channel P2rX4 to sense extracellular ATP (eATP) released by BM osteoblasts via the gap junction protein Pannexin 3 (Panx3). Mutation of Panx3 or P2rX4 each caused decreased serum antibodies and selective loss of BM PCs. Compared to their WT counterparts, Panx3-null osteoblasts secreted less eATP and failed to support PCs *in vitro*. The P2rX4-specific inhibitor 5-BDBD abrogated the impact of eATP on BM PCs *in vitro*, depleted BM PCs *in vivo* and reduced pre-induced antigen-specific serum antibody titers with little post-treatment rebound. P2rX4 blockade also reduced autoantibody titers and kidney disease in two mouse models of humoral autoimmunity. P2rX4 promotes PC survival by regulating ER homeostasis, as short-term P2rX4 blockade caused accumulation of ER stress-associated regulatory proteins including ATF4, and B-lineage mutation of the pro-apoptotic ATF4 target CHOP prevented BM PC demise upon P2rX4 inhibition. Thus, generating mature protective and pathogenic PCs requires P2rX4 signaling controlled by Panx3-regulated eATP release from BM niche cells.

[‡]Address correspondence to: Masaki Ishikawa (masaki.ishikawa@pennmedicine.upenn.edu) David Allman (dallman@pennmedicine.upenn.edu), or Avinash Bhandoola (avinash.bhandoola@nih.gov).

Author contributions

M.I., D.A. and A.B. designed the experiments. M.I., Z.H., Y.Z., A.D., C.R. and J.L. performed the experiments including all ELISPOT, ELISA and flow cytometry studies. M.L. performed bioinformatic analyses. M.I., D.A. and A.B. wrote the manuscript with input from all other co-authors.

Competing interests

The authors have no competing financial interests.

Keywords

Pannexin 3; P2rX4; plasma cell; bone marrow niche

Purinergic receptors of the P2rX family are ligand-gated cation channels that interpret the microenvironmental release of ATP[2]. Within the immune system, P2rX receptors can augment innate and adaptive immunity by sensing the uncontrolled release of ATP by infected or dying cells[3,4]. By contrast, gap-junction proteins such as Panx3 control the regulated release of ATP by developing and mature BM osteoblasts[5]. We analyzed hematopoietic and immune cell populations in Panx3$^{-/-}$ mice, which have reduced BM cellularity because they have shorter bones with narrower medullary cavities, but otherwise display relatively intact BM architecture[6]. Consistently, numbers of developing BM myeloid and B cell precursors, including immature and mature B cells, were reduced by 50–70% (Extended Data Fig. 1a,b). We observed minimal impact on developing T cells in the thymus, B and T cells in the spleen, or peritoneal cavity B1 B cells. (Extended Data Fig. 1c–e, see Extended Data Figs. 2 and 3 for flow cytometric gating strategies for BM PCs and precursor populations, and activated splenic B cells). However, serum IgG, IgM and IgA titers were reduced substantially in Panx3$^{-/-}$ mice (Fig. 1a), and ELISPOT analyses revealed far fewer IgG- and IgM-secreting PCs among BM but not spleen cells from Panx3$^{-/-}$ mice (Fig. 1b). Furthermore, BM PCs identified by surface co-expression of CD138 and Sca-1[7] were reduced profoundly in Panx3$^{-/-}$ mice (Fig. 1c). CD138^{high} Sca-1^{+} BM PCs include newly generated antibody-secreting cells identified by surface B220 expression, as well as a B220^{-} population enriched for mature long-lived PCs (LLPCs)[8], and both BM PC subsets were compromised by Panx3 mutation (Extended Data Fig. 1f). In sharp contrast, frequencies and numbers of splenic PCs were unchanged (Extended Data Fig. 1g). Therefore, Panx3 promotes the generation and/or maintenance of mature BMPCs.

Because Panx3 is expressed chiefly by osteoblasts[5], we induced osteoblast differentiation from calvarial cells from WT and Panx3$^{-/-}$ mice, and established co-cultures with these osteoblasts and BM cells from WT or Panx3$^{-/-}$ mice (see Extended Data Fig. 4a). Four days later we performed ELISPOT assays to quantify PCs, and noted far fewer IgG-secreting cells when WT BM cells were cultured on Panx3$^{-/-}$ osteoblast feeder cells compared to all other combinations (Fig. 1d). Of note, numbers of PCs recovered from BM cells cultured with WT osteoblasts mirrored PC numbers on day zero (Fig. 1d). Whereas CXCL12, SCF, IL-6 and APRIL can each support PC survival[9], we found no differences in mRNA abundance for each in induced WT and Panx3$^{-/-}$ osteoblasts (Extended Data Fig. 4b). However, supernatants of Panx3$^{-/-}$ osteoblasts contained reduced eATP levels (Fig. 1e), raising the possibility that osteoblasts support PCs by using Panx3 to release eATP. Consistent with this possibility, adding ATP but not ADP or AMP without osteoblastic feeders drove recovery of PCs from WT BM cells to levels in line with PC numbers observed on day zero (Fig. 1f). Similarly, eATP addition also promoted recovery of the small numbers of PCs available in Panx3$^{-/-}$ BM cells, again to levels identified on day zero (Fig. 1f). Together, these data suggest that Panx3-regulated eATP release modulates BM PC function and/or survival with a lesser role for PCs outside the BM.

P2rX receptors include seven different family members with different expression patterns. To test for a role for P2rX receptors in BM PCs, we first treated mice with the global P2rX inhibitors suramin or PPADS[10,11]. Whereas suramin is less effective at inhibiting P2rX4 function[12], both suramin and PPADS reduced frequencies of $CD138^{high}$ $B220^{-}$ BM cells with the phenotype of PCs *in vivo* (Extended Data Fig. 5a). Available RNAseq data indicate that among P2rX family members P2rX4 is highly expressed by mouse BM PCs, and is also expressed by human BM PCs (Extended Data Fig. 5b,c)[13,14]. Thus, we mutated P2rX4 in B-lineage cells by crossing $P2rX4^{fl/fl}$ mice with mice harboring either an Mb1-Cre allele for mutation in early B cell precursors[15] or a CD20-regulated tamoxifen induced Cre-ERT2 BAC transgene ("CD20-TAM-Cre") for induced mutagenesis in mature B cells[16].

Steady state serum Ig titers and both $B220^{+}$ and $B220^{-}$ BM PCs were significantly reduced in $P2rX4^{fl/fl}$;Mb1-Cre mice compared to $P2rX4^{+/+}$;Mb1-Cre controls (Fig. 2a,b, Extended Data Fig. 6a). ELISPOT assays revealed that IgG- and IgM-secreting cells were reduced substantially in BM but not spleen in $P2rX4^{fl/fl}$;Mb1-Cre adults (Fig. 2c). By contrast, frequencies of naïve B cells in the spleen, developing B-lineage cells in the BM, and peritoneal cavity B1 B cells were minimally changed (Extended Data Fig. 6b–d). Consistent with the notion that BM PCs use P2rX4 to sense eATP, adding eATP augmented numbers of IgG-secreting cells in short-term cultures of $P2rX4^{+/+}$;Mb1-Cre but not $P2rX4^{fl/fl}$;Mb1-Cre BM cells (Fig. 2d). In parallel we fed $P2rX4^{fl/fl}$;CD20-TAM-Cre and $P2rX4^{+/+}$;CD20-TAM-Cre mice tamoxifen-laced chow for 4 weeks beginning at 5 weeks of age. This strategy also caused a 2–3-fold decrease in steady state serum Ig titers (Fig. 2e). Additionally, delivery of tamoxifen in this fashion to $P2rX4^{fl/fl}$;CD20-TAM-Cre and $P2rX4^{+/+}$;CD20-TAM-Cre mice beginning at 12 weeks of age caused substantial loss of the bulk of steady state BM PCs (Fig. 2f), and equally compromised both $B220^{+}$ and $B220^{-}$ PCs in the BM without affecting numbers of steady state PCs in the spleen and with minimal effects on naïve and developing B-lineage cells (Extended data Fig. 6e–g). ELISPOT analyses of cultured BM cells confirmed that tamoxifen-pulsed $P2rX4^{fl/fl}$;CD20-TAM-Cre mice possessed reduced numbers of PCs, even with addition of eATP (Extended Data Fig. 6h). We conclude that BM PCs critically depend on P2rX4.

The impact on steady state numbers of BM PCs in $P2rX4^{fl/fl}$;CD20-TAM-Cre mice was perhaps surprising given that PCs are not reduced dramatically in mice given anti-CD20 antibodies[17]. Because BAC transgene expression can extend beyond prescribed cell- and stage-restricted expression patterns and levels[18], we probed for Cre protein expression and evidence of P2rX4 mutation in mature BM PCs. As shown, the Cre protein was readily detected by flow cytometry in mature $B220^{-}$ BM PCs from CD20-TAM-Cre adults (Extended Data Fig. 7a). Likewise, using a genomic PCR assay we observed evidence for P2rX4 mutation among BM $B220^{-}$ PCs that remained in $P2rX4^{fl/fl}$;CD20-TAM-Cre mice after pulsing with tamoxifen for only 7 days (Extended Data Fig. 7b). We conclude that CD20-TAM-Cre mice are a model for inducible mutagenesis in BM PCs, in addition to their known utility for studies of splenic naïve B cells and germinal center (GC) B cells[16]. Further, these results are consistent with the idea that P2rX4 is required by established BM PCs to persist in the BM.

To examine antigen-specific PCs, we fed P2rX4$^{fl/fl}$;CD20-TAM-Cre and control P2rX4$^{+/+}$;CD20-TAM-Cre mice with tamoxifen-laced chow for 4 weeks, then immunized these mice with the T cell dependent hapten-carrier (4-hydroxy-3-nitrophenyl)acetyl-Keyhole Limpet Hemocyanin (NP-KLH). We quantified NP-specific PCs in the spleen on day 7 and day 30, and the BM at day 30 post-immunization by ELISPOT. For P2rX4$^{fl/fl}$;CD20-TAM-Cre mice numbers of NP-specific PCs were reduced substantially in the BM at day 30, but not the spleen at either day 7 (Fig. 2g), or day 30 (Extended Data Fig. 7c). Additionally, P2rX4$^{fl/fl}$;CD20-TAM-Cre mice showed no reduction of NP-specific splenic GC B cells (Extended Data Fig. 7d). We conclude that P2rX4 is required to establish BM PC populations to an exogenous antigen.

We next evaluated the impact of the P2rX4 specific inhibitor 5-BDBD. In short-term BM cultures, baseline numbers of antibody secreting cells and the capacity of eATP to sustain PC numbers were both abolished by 5-BDBD but not by the P2rX7 inhibitor A438079 (Fig. 3a). Further, treatment of WT mice with 5-BDBD significantly reduced numbers of BM PCs including B220^{-} CD138^{+} LLPCs (Fig. 3b and Extended Data Fig. 8a), without affecting numbers of steady state splenic PCs or naïve B cells or CD4^{+} and CD8^{+} splenic T cells in unimmunized mice (Extended Data Fig. 8b,c), or NP-specific GC B cells in NP-KLH immunized mice (Extended Data Fig. 8d).

We also examined the impact of 5-BDBD on serum antibody titers in WT mice that were previously immunized with NP-KLH. We delivered 5-BDBD to WT adults immunized with NP-KLH 60 days previously, using Panx3$^{-/-}$ mice as additional controls. Serum NP-specific IgM and IgG titers were each severely reduced by 5-BDBD, and remained reduced for at least 80 days after terminating 5-BDBD treatments (Fig. 3c). As expected hapten-specific antibodies were highly compromised across all time points in Panx3$^{-/-}$ mice, with no further effect of P2rX4 inhibition by 5-BDBD (Fig. 3c).

We evaluated two models of systemic lupus erythematosus (SLE) characterized by serum antibodies against double stranded DNA (dsDNA) and progressive proteinuria. NZB/W mice experience a spontaneous and progressive age-associated disease beginning at 20 weeks of age[19]. Treatment of NZB/W mice with 5-BDBD beginning at 29 weeks-of-age caused robust arrest in IgG anti-dsDNA titers and a precipitous drop in overall proteinuria (Fig. 3d,e). In NZB/W mice 5-BDBD also arrested age-associated increases in urine albumin levels (Fig. 3f), and other disease indicators including kidney hypopigmentation and renal tubular hypertrophy with large hyaline casts (Fig. 3g). Additionally, we induced anti-dsDNA antibodies and proteinuria in B6 mice by transferring B6.H2-Ab1^{bm12} splenocytes[20]. Similar to our observations in NZB/W mice, 5-BDBD administration reduced pre-established proteinuria and arrested anti-dsDNA IgG titers when administered beginning 5 weeks after transfer of B6.H2-Ab1^{bm12} splenocytes (Fig. 3h,i). Consistent with the conclusion that P2rX4 inhibition severely depletes mature BM PCs, rebound kinetics of anti-dsDNA antibody serum titers and proteinuria were relatively slow compared to the rapid rebound observed in NZB/W mice given the mTOR inhibitor rapamycin which arrests antibody synthesis in mature BM PCs without causing their demise (Fig. 3d,e,h,i, Extended Data Fig. 9)[8]. We conclude that short-term P2rX4 inhibition causes loss of pathogenic antibody titers by depleting BM PCs.

Because P2rX receptors are nonselective channels for Ca^{2+} and other cations needed for optimal ER function[21], we considered the possibility that eATP/P2rX4 signaling promotes endoplasmic reticulum (ER) homeostasis in BM PCs. Robust sustained antibody synthesis requires the ER sensor IRE1α, which activates the unfolded protein response (UPR) by splicing nascent RNA transcripts encoded by the Xbp1 gene to encode a functional transcription factor termed Xpb1s[22]. We witnessed increased levels of Xpb1s and the additional UPR-affiliated transcriptional regulator ATF4[22] in BM LLPCs 24 hours after delivering a single dose of 5-BDBD to WT adults (Fig. 4a,b). Hyperacute ER stress can induce apoptosis by causing ATF4 to promote expression of the transcription factor CCAAT/enhancer-binding protein-homologous protein (CHOP)[23] which then drives transcription of the proapoptotic Bcl-2 family member Bim[24]. We therefore questioned whether P2rX4 inhibition causes BM PC depletion by unleashing the ATF4-CHOP pathway. To test this hypothesis, we evaluated the impact of 5-BDBD on PCs in $CHOP^{fl/fl}$;CD20-TAM-Cre and control $CHOP^{+/+}$;CD20-TAM-Cre adults that were fed tamoxifen for 4 weeks before immunizing with NP-KLH. ELISPOT analysis (Fig. 4c,d) revealed that CHOP mutation prevented 5-BDBD-mediated depletion of IgG secreting BM LLPCs, including NP-specific BM PCs in mice that were immunized 4 weeks previously and 14 days after terminating tamoxifen delivery. We confirmed that 4 weeks tamoxifen exposure was sufficient to induce CHOP mutation in B cells and BM PCs but not T cells of $CHOP^{fl/fl}$;CD20-TAM-Cre young adults (Extended Data Fig. 10). We conclude that P2rX4 inhibition causes an acute ER stress response that initiates a CHOP-dependent death pathway in BM PCs.

DISCUSSION

Our experiments show that establishing and maintaining optimal serum antibody titers requires activation of the purinergic receptor and cation channel P2rX4 on PCs. Our results further suggest that BM PCs including LLPCs use P2rX4 to avoid ER-regulated apoptosis by recognizing the homeostatic release of eATP by Panx3-expressing osteoblastic niche cells. Mutation of P2rX4 in developing B-lineage cells using Mb1-Cre resulted in reduced serum antibody titers and greatly reduced numbers of BM PCs, indicating that P2rX4 is required to establish normal BM PC populations. Moreover, induced mutation of P2rX4 in B cells and plasma cells using CD20-TAM-Cre reduced serum antibody titers to a comparable degree, and greatly depleted BM PCs, including the $B220^{-}$ fraction that is enriched for mature LLPCs. It is therefore likely that most BM-resident PCs including LLPCs depend on P2rX4. In each setting, other aspects of B cell development including induction of GC B cells and splenic PCs were unaffected. Further, eATP release by osteoblasts and their capacity to support PC function in vitro was compromised by Panx3 mutation, and the ability of eATP to support PCs in vitro was abrogated by arresting P2rX4 function with 5-BDBD. Thus, BM PCs sense eATP via P2rX4. Our results support the conclusion that Panx3-dependent release of eATP by osteoblastic BM cells and its detection by P2rX4 on PCs are essential events defining BM niches for PCs.

How mature PCs avoid apoptosis to sustain serum antibody titers remains poorly understood. A widely accepted model holds that mature PCs must localize to specialized BM survival niches orchestrated by the chemokine CXCL12[25]. However, the identity of all relevant niche-associated survival factors remains uncertain, and plasma cell lifespan

may also be affected by additional cell-intrinsic pathways[26]. One key cell extrinsic factor is the cytokine APRIL, which delivers anti-apoptotic signals to PCs by binding to the surface receptor BCMA[27,28]. Indeed, BCMA mutant mice possess only residual numbers of BM PCs in a manner similar to Panx3 mutants as well as mice harboring P2rX4-mutant B-lineage cells[29]. However, BM PC numbers are unaffected by APRIL mutation without concomitant depletion of the cytokine BAFF, an alternative BCMA ligand[27]. Because BAFF is available outside the BM including in serum[30,31], PC access to BAFF and perhaps APRIL is unlikely to be restricted to BM PC niches. In contrast, our results point to Panx3-regulated eATP release by osteoblastic lineage cells and its interpretation by P2rX4 on PCs as a defining and unique feature of PC survival niches within the BM.

Within the immune system eATP is often viewed as a pro-inflammatory signal that opens P2rX channels such as P2rX7 to trigger or augment macrophage and memory T cell function in response to infection and tissue injury[3,32]. In contrast, our results reveal that PCs use P2rX4 to sense the regulated homeostatic release of eATP within non-inflammatory microenvironments in the BM. This idea is consistent with the observation that P2rX4 possesses a uniquely high binding affinity for eATP among P2rX receptors[33], and other work proposing that pro-inflammatory events are actively suppressed in the BM as a strategy to protect specialized niches, including those harboring mature PCs[34,35]. Thus, our findings suggest that P2rX receptors have evolved to interrogate eATP levels to regulate a diverse array of cell fates, including within the immune system.

Our work also identifies P2rX4 as a key upstream regulator of ER function, as short-term P2rX4 blockade caused rapid activation of the IRE1-Xbp1 pathway and increased abundance of the additional UPR regulator ATF4 in BM PCs. An intimate relationship between P2rX4 and the ER is further indicated by the capacity of CHOP mutation to rescue BM PCs experiencing P2rX4 inhibition, as CHOP is known to mediate apoptosis due to acute or unresolved ER stress[36]. In this regard, the lack of impact of P2rX4 blockade on antibody-secreting PCs in the spleen was perhaps surprising. One possible explanation for these data centers on previous results indicating that newborn PCs experience progressive increases in immunoglobulin synthesis which in turn causes stepwise increases in UPR activity[37]. Therefore, relatively immature PCs such as those in the spleen may be intrinsically less sensitive to P2rX4 inhibition. Given that small numbers of PCs can persist in the spleen for at least several months post-induction without input from activated B cells[38], it may be informative to learn if PCs that persist outside the BM for extended periods eventually become susceptible to P2rX4 blockade. Alternatively, PCs in spleen and BM may depend on different signals to regulate the UPR.

PCs play roles in a broad range of afflictions ranging from antibody-mediated autoimmunity and transplant rejection to multiple myeloma, an incurable malignancy of BM PCs. Our results demonstrate that the P2rX4 inhibitor 5-BDBD can be used to deplete BM PCs and substantially reduce pre-existing serum antibody titers, including for autoantibodies generated in two different mouse models of autoimmune disease. Treatment of previously immunized mice with 5-BDBD caused rapid and sustained loss in pre-established serum antibodies, and delivery of 5-BDBD to disease-prone NZB/W mice reduced lupus-affiliated symptoms including urine albumin and overall proteinuria, and prevented several additional

metrics of kidney disease. Current strategies for eliminating problematic PCs mainly target processes unique to PC biology survival and function. These include bispecific antibodies or engineered patient T cells targeting BCMA[39,40], and proteasome inhibitors intended to induce a terminal ER stress response due to perturbed proteostasis in normal and malignant LLPCs[41–43]. Given that 5-BDBD increased intracellular abundance of XBP1s and ATF4 and caused CHOP-dependent LLPC depletion, we suggest that the eATP/P2rX4 pathway may prove useful as an alternative strategy to induce hyperacute ER stress and apoptosis in problematic LLPCs in autoimmunity and other settings. Ultimately, for humoral autoimmunity and allo-antibody producing cells such strategies will dovetail with approaches that target antigen-specific PCs[44] to avoid depleting PCs producing beneficial antibodies. In addition, given the capacity of eATP to sustain numbers of antibody secreting cells in culture, we speculate that the insights from the present study will illuminate pathways leading to new methods to increase protective antibody titers.

Methods

Mice

C57BL/6 (B6), B6.Mb1-Cre (B6.C(Cg)-*Cd79a*$^{tm1(cre)Reth}$/EhobJ), B6.H2-Ab1^{bm12}, NZB/W and CHOP$^{+/fl}$ mice were obtained from the Jackson Laboratory (Bar Harbor, ME) and bred and/or maintained in our colonies at the University of Pennsylvania and/or the NCI. Panx3 KO mice were provided by Y. Yamada[6] (National Institutes of Health, Bethesda, Maryland, USA) and housed in our NCI colony. P2rX4$^{fl/fl}$ (P2rx4$^{tm1c(EUCOMM)Wtsi}$) mice were obtained from the MRC Harwell Institute (Oxfordshire, UK) and re-derived at the NCI (Frederick, Maryland, USA). Human CD20 (hCD20) transgenic mice containing an internal ribosomal entry site (IRES)-ERT2Cre in the 3′-UTR of the hCD20 gene (hCD20-TAM-Cre)[16] were provided by M.J. Shlomchik (University of Pittsburgh, Pittsburgh, PA, USA). All mice were used at 8–12 weeks of age unless otherwise indicated.

Immunizations and treatments

Mice were immunized i.p. with 50 μg NP_{18}-KLH in alum. To induce Cre activity, adults were fed tamoxifen-laced cow (ENVIGO) for 4 weeks before initiating experiments. Mice were treated with 5-BDBD (4.25 mg/kg i.v.; R&D), Suramin (2.0 mg/kg i.v.; Abcam), or PPADS (2.5 mg/kg i.v.; Santacruz)[45] in a volume of 30μl. 5-BDBD and the P2rX7 inhibitor A438079 (R&D Systems) were each used in vitro at a final concentration of 50μM. All P2rX inhibitors were dissolved initially in DMSO.

Flow cytometry

BM cells were flushed from femurs, tibiae and ilia using a 27-gauge needle and spleens were mechanically disrupted using frosted microscope slides. BM cells and splenocytes were stained and analyzed in FACS buffer (PBS containing 0.1% sodium azide, 1 mM EDTA, and 0.5% BSA). Cells were counted using a Cellaca MX cell counter (Nexcelom Biosciences). Antibodies specific for CD4 (RM4-4), CD8α (53–6.7), TER-119 (TER-119), F4/80 (BM8), B220 (RA3–6B2), CD19 (1D3), CD138 (300506), CD38 (90), IgD (11–26c), GL7 (GL-7), AA4.1 (R3), IgM (II/41), CD43 (84–3C1), TCRβ (H57–597), CD25 (PC61.5), CD44 (IM7), CD62L (MEL-14), CD11b (M1/70), and Streptavidin APC-eFluor™ 780 were

from eBioscience. ATF4 (CL594–60035) was from Proteintech. XBP1s (Q3–695), CD5 (53–7.3), and CD43 (S7) were from Becton Dickinson. All Dump channels consisted of antibodies to CD4, CD8, TER-119, and F4/80. Non-viable cells were identified using the violet-excited Zombie aqua fixable dye (BioLegend). To evaluate intracellular Cre expression, surface-stained cells were fixed for 5 min with 10% formalin, washed, then incubated for 30 min in BD Phosflow Perm Buffer III (BD Biosciences). Cells were then washed and then stained for 30 min with a PE-conjugated rabbit anti-Cre antibody (Cell Signaling Technology). Samples were acquired using a LSR Fortessa or Symphony A3 lite flow cytometer (Becton Dickinson) using FACSDiva v9.1 and analyzed using FlowJo software (Tree Star). All analyses were first gated on viable singlet cells.

Osteoblast cultures

Calvaria were digested six times for 10 min by 0.1% collagenase type 1 (Worthington Biochemical Corp.) and 0.2% dispase II (Roche) in PBS. The last two fractions were collected in culture medium consisting of α-minimum essential medium (Invitrogen) with 10% FBS, 100 U/ml of penicillin, and 100 μg/ml of streptomycin. For the co-culture assay, primary calvarial cells were induced by the addition of 50 μg/ml ascorbic acid (Sigma-Aldrich) and 5 mM β-glycerophosphate (Sigma-Aldrich) for 14 days before co-culture experiments.

ELISPOT and ELISA

ELISPOT assay was determined by Mouse IgG ELISpot kit (Mabtech). In brief, plates (Millipore) were coated with NP_4-BSA, anti–H+L Ig (all 15 μg/ml) or dsDNA (10 μg/ml) in sodium bicarbonate buffer. Unless indicated otherwise, for ELISPOT analyses we plated 10^6 cells/well unless cells were taken from earlier cultures that were also initiated with 10^6 cells per well. Plates were blocked overnight with RPMI with 10% FBS. Plates were washed using PBS with 0.1% Tween 20, followed by incubation with biotinylated anti-IgG antibodies (Mabtech). Biotinylated antibodies were revealed using streptavidin-HRP (Mabtech), and spots visualized with TMB (Mabtech). Wells were imaged using ImmunoSpot software (Cellular Technology) and manually counted using Fiji (ImageJ) software. Background wells used no cells and contained 0–1 spots. ELISA for total serum IgG, IgM, and IgA was performed with ELISA kit (Thermo) according to the manufacturer's instructions. In brief, diluted sera was applied to antigen-coated 96-well plates. Primary antibodies were detected with horseradish peroxidase–conjugated anti-IgG, anti-IgM, or anti-IgA secondary antibodies (Thermo), followed by incubation with TMB substrate. ELISA analyses for NP-specific serum antibodies were performed with NP_{26}-BSA (Biosearch Technologies) coated plates and ELISAs for dsDNA antibody titers were performed with a Mouse anti-DNA antibody ELISA Kit (Abcam).

Urine protein and albumin analyses

Proteinuria in NZB/W and B6.H2-$Ab1^{bm12}$ mice was measured using Albustix Urinalysis Test Strips (Siemens) according to the manufacturer's instructions. Briefly, fresh urine was applied to reagent strips and the colorimetric change determined using the following scale: 1≥, 30 mg/dl protein; 2≥, 100 mg/dl; 3≥, 300 mg/dl; and 4≥, 2,000 mg/dl. Urine

albumin levels were determined with a mouse albumin ELISA Kit (Abcam) according to the manufacturer's instructions.

Histological analyses

Kidney samples were fixed in 4% paraformaldehyde and embedded in paraffin wax. After deparaffinization and rehydration, sions were stained with Hematoxylin & Eosin or Periodic Acid-Schiff (PAS) reagent with the assistance of the Penn Vet Comparative Pathology Core.

ATP flux

ATP flux was examined by luminometry, as previously described[5,46]. Primary calvarial cells isolated from Panx3 KO mice were seeded at 10^4 cells/well in a 96-well plate, and induced by osteogenic culture media for 14 days. The cells were then washed with PBS, followed by incubation in PBS for 2 min. The supernatant was collected and assayed with luciferase and luciferin (Promega). The luminescence was measured using an Infinite 200 PRO (TECAN).

Statistics

Statistical differences between two groups were evaluated using the two-tailed non-parametric Mann-Whitney U test. For analyses involving multiple time points per group, a repeated measures ANOVA was used with correction for multiple comparisons using the original method of Benjamini and Hochberg, with a desired false discovery rate of 0.05. All statistics were performed in Prism software (version 9.51, GraphPad).

Bioinformatics

Publicly available BM scRNAseq data[14] were downloaded in h5ad format from the Chan-Zuckerberg CellxGene website and loaded into python 3.9 using SCANPY (version 1.9.3)[47]. Batch correction was performed by selecting 2000 highly variable genes[48], taking the different sequencing assays into account and fed into scVI (single-cell variational inference)[49], with n_layers set to 2, n_latent set to 30 and gene likelihood set to negative binomial. Latent dimensions were used to identify clusters using the Leiden algorithm[50]. B cell lineage cells were isolated based on their cluster identity and published annotation. This subset was reanalyzed in the same fashion, followed by gene expression data normalization, log transformation. A UMAP manifold was computed on the latent dimensions obtained from scVI.

Study approval

All animal studies described herein were reviewed and approved by the National Cancer Institute ACUC or the University of Pennsylvania IACUC. Animals were bred and maintained in accordance with institutional guidelines for animal welfare.

Extended Data

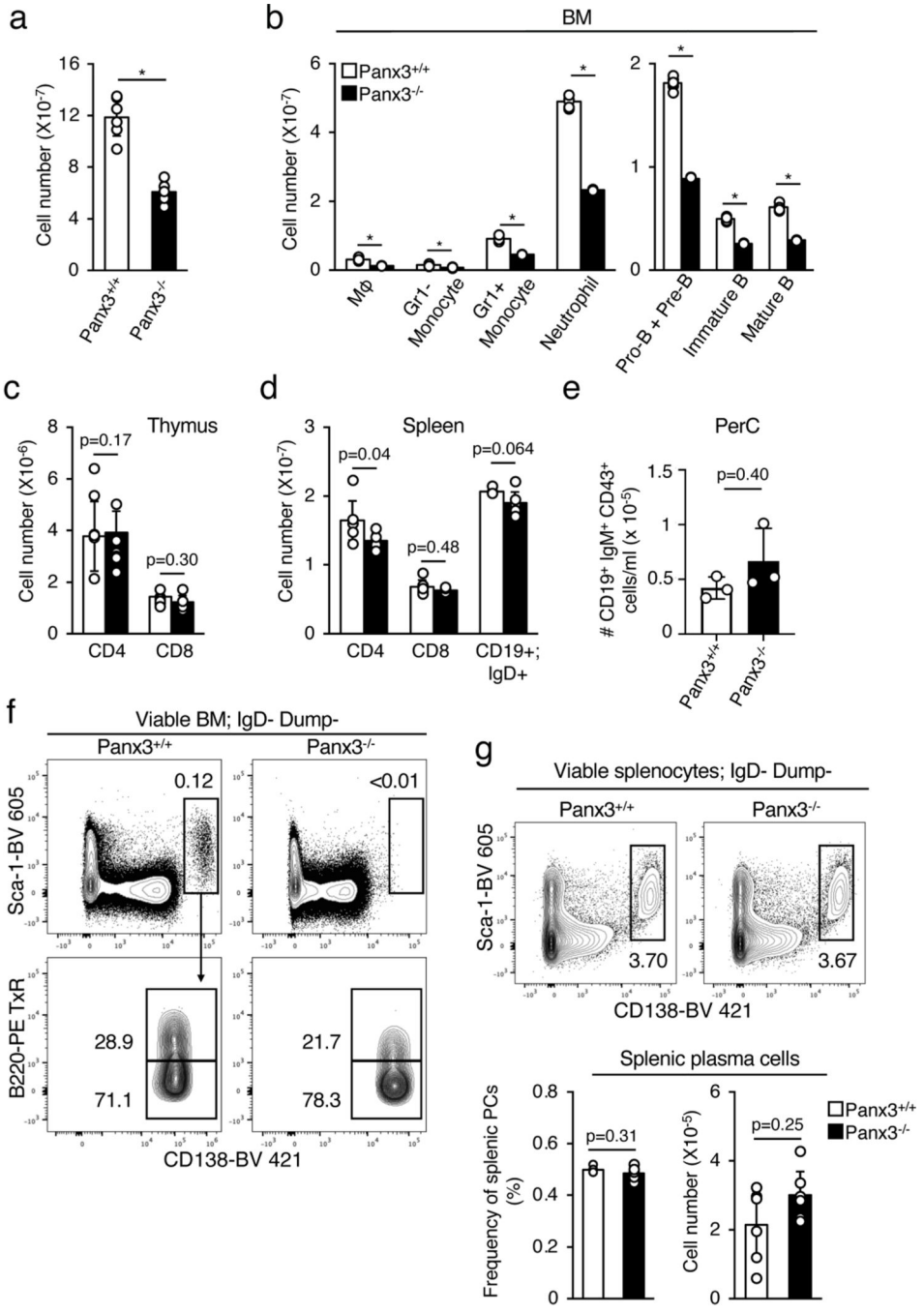

Extended Data Figure 1. Panx3 mutation does not perturb developing or mature myeloid and lymphoid cell populations.

(a) Numbers of viable BM cells in 16-week-old Panx3$^{+/+}$ and Panx3$^{-/-}$ mice. (b-e) Evaluation of the indicated BM myeloid and B-lineage cells (b), thymocytes (c), T and B cells in spleen (d) and peritoneal B1 cells (e). (b) Numbers of macrophages (CD115^{-} Gr1^{-} F4/80^{+}), Gr1^{+} and Gr1^{-} monocytes (CD115^{+} Gr1^{high}, CD115^{-} Gr1^{low} F4/80$^{+/-}$ respectively), neutrophils (CD115^{-} Gr1^{high}), pro- & pre-B cells (CD19^{+} IgM^{-} CD43$^{+/-}$),

and immature ($CD19^+$ IgM^+ IgD^-) and mature ($CD19^+$ IgM^+ IgD^+) B cells. (c-e) Numbers of CD4 and CD8 single positive thymocytes (c), splenic CD4 and CD8 T cells and mature ($CD19^+$ IgD^+) B cells (d), and peritoneal cavity CD19+ CD43+ B1 B cells (e) in 5-month-old $Panx3^{+/+}$ and $Panx3^{-/-}$ mice. (See Extended Figs. 2 and 3 for flow cytometry gating strategies for BM and spleen cells). (n=6/grp for panels a-d, n=3/grp for panel e). (f, g) $CD138^+$ $Sca\text{-}1^+$ PCs in the BM (f) and spleen (g) in 16-week-old $Panx3^{+/+}$ and $Panx3^{-/-}$ mice (n=6/grp). Plots in (f) show additional analysis of newly formed ($B220^+$) and mature ($B220^-$) PCs. All bar graphs are means. For panels (a,b), *, $p = 0.0022$. All p values were derived from two-tailed Mann-Whitney tests, without any adjustment for multiple comparisons. The experiments in panels (a-d) and (f-g) were performed at least thrice and the experiments in panel (e) were performed twice.

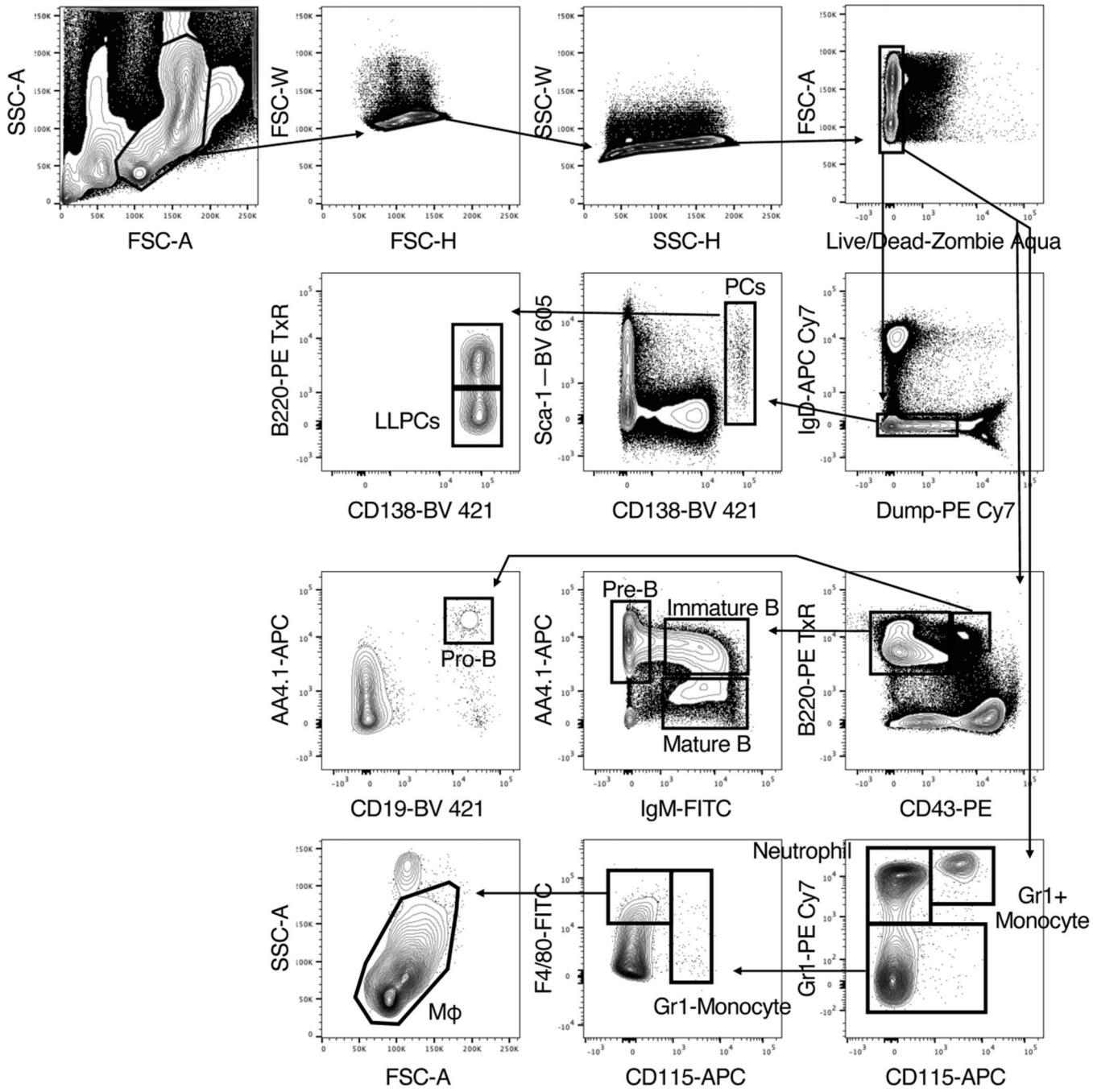

Extended Data Figure 2. Gating strategy for BM analysis.

Gating strategy for flow cytometric analysis of BM cells related to Figure 1c, 2b, 2f, 3b, 4a, 4b and Extended Data Figure 1f, 5a, 6a, 6e, 7a, 8a.

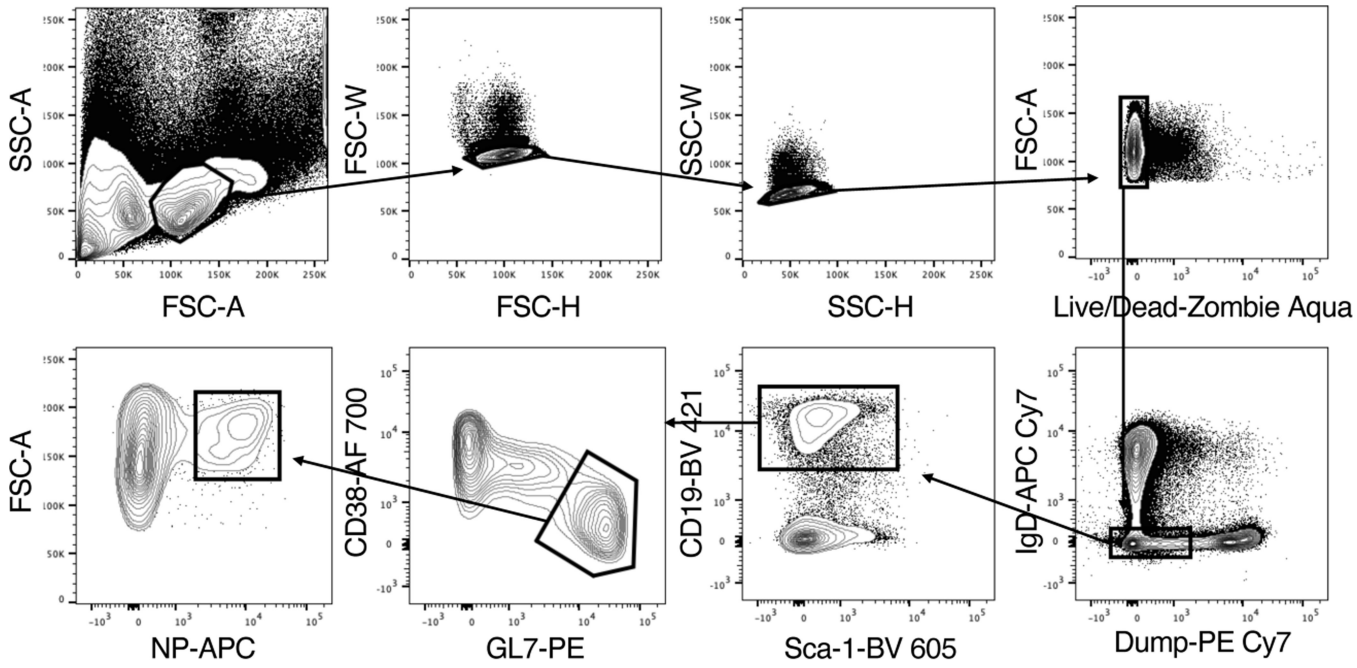

Extended Data Figure 3. Gating strategy for spleen analysis.

Gating strategy for flow cytometric analysis of splenocytes related Extended Data Figure 7d, 8d.

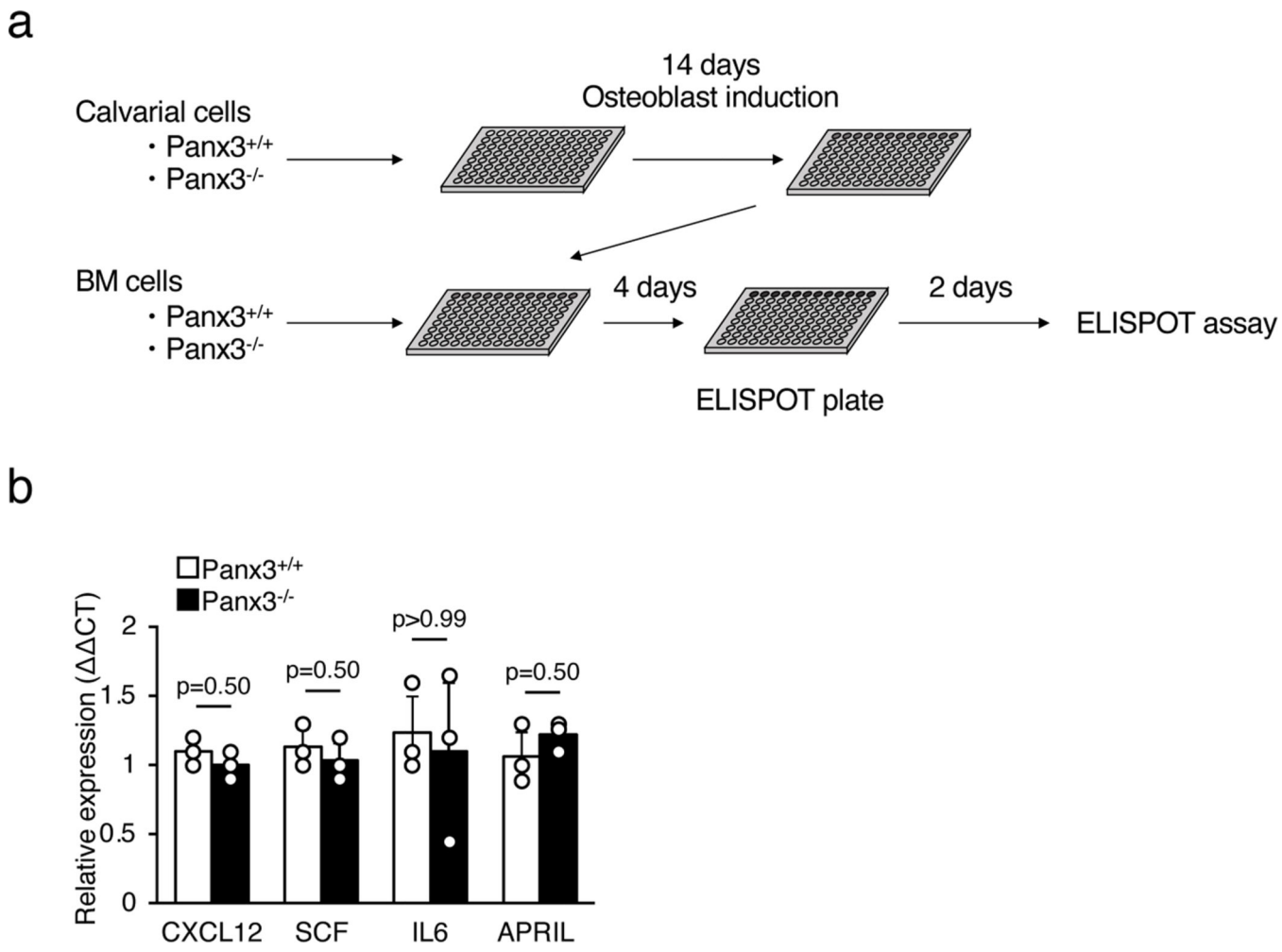

Extended Data Figure 4. Panx3 and eATP support BM PCs.

(a) Schematic for experiments wherein fresh BM cells were cultured with pre-induced osteoblastic cells for 4 days before ELISPOT analyses. (b) Quantitative RT-PCR for CXCL12, SCF, IL6 and APRIL expression with osteoblastic calvarial cells from $Panx3^{+/+}$ and $Panx3^{-/-}$ mice after 14 days culture as in (a). Graph shows means for technical replicates; $n = 3$. A control $Panx3^{+/+}$ sample was set to 1 for each set of measurements, and the other measurements were recalculated relative to that sample. All p values were derived from two-tailed Mann-Whitney tests, without any adjustment for multiple comparisons. The experiments in panel b were performed twice.

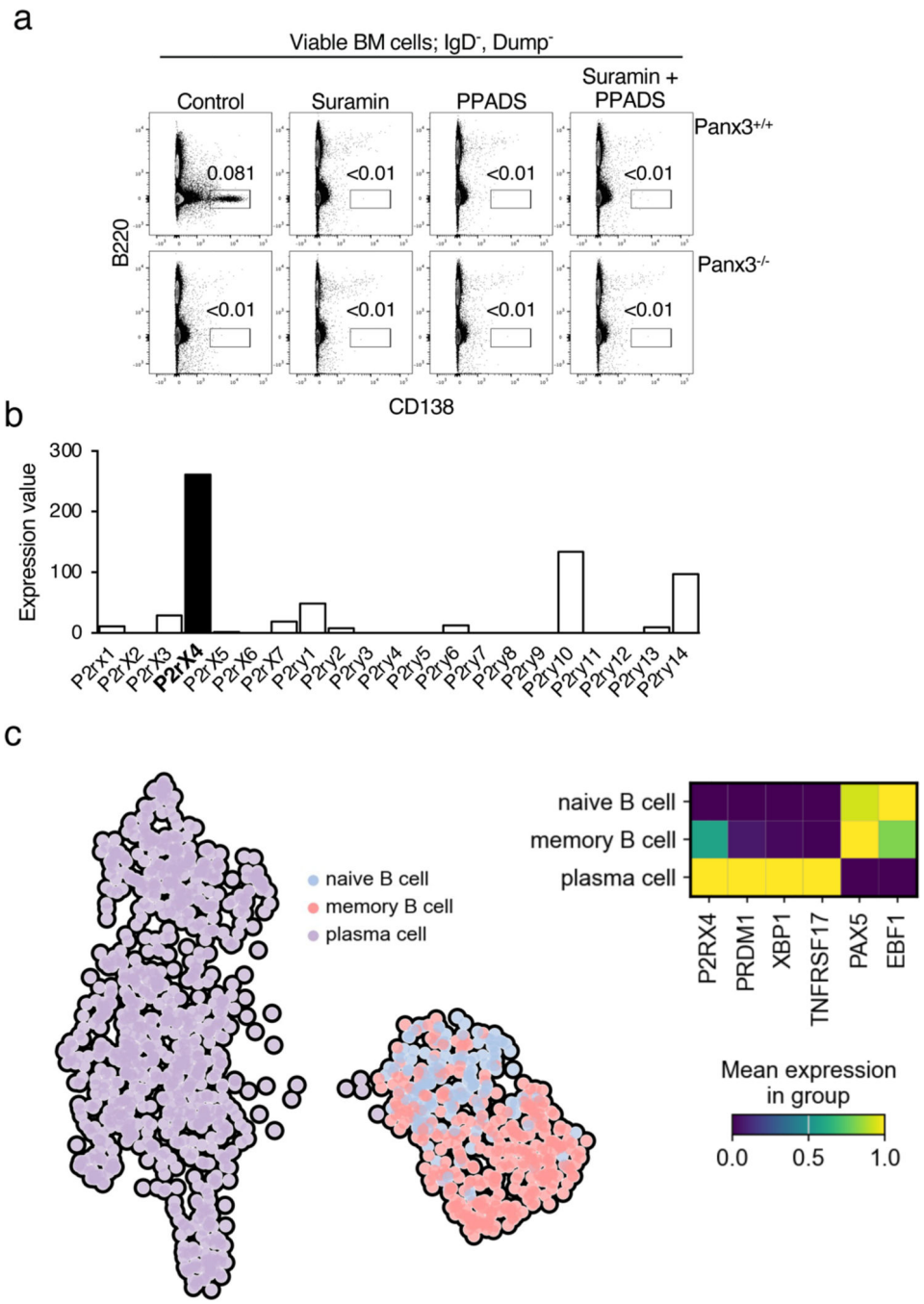

Extended Data Figure 5. P2rX inhibitors deplete BM PCs.

(a) Representative flow cytometry data for BM PCs in WT mice given DMSO alone (Control) or Suramin (2.0 mg/kg), PPADS (2.5 mg/kg), or both Suramin and PPADS thrice over seven days before analysis. Representative of 3 mice per group and three separate experiments. (b) Expression of P2rX and P2rYfamily members in BM PCs (ImmGen data, see Methods). (c) Annotated UMAP visualizing naïve and memory B cells and plasma cells identified in adult human bone marrow (left) with Heatmap visualizing averaged and gene-wise scaled gene expression for each population (right) (see Methods).

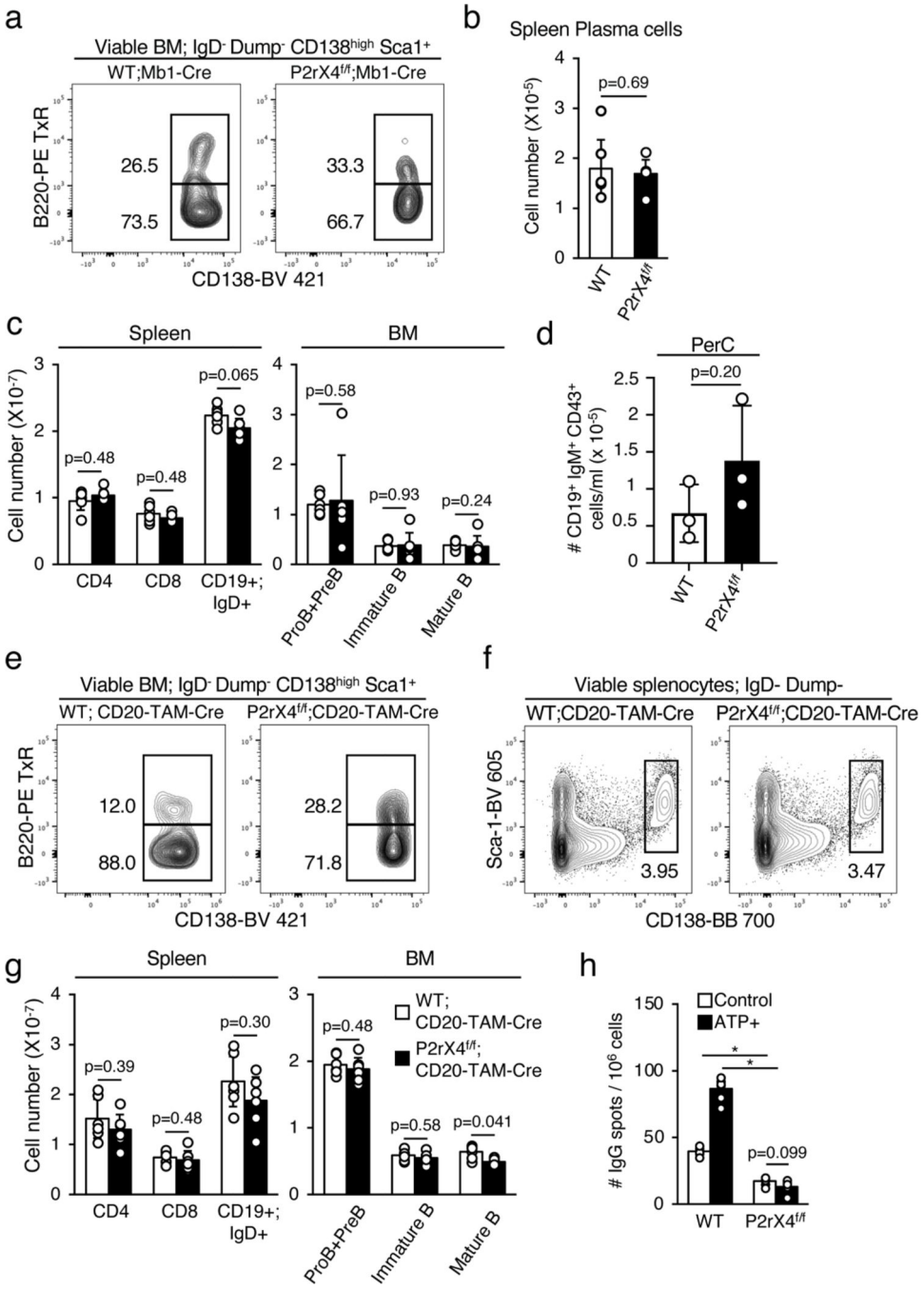

Extended Data Figure 6. Selective impact of B-lineage P2rX4 mutation on BM PCs.

(a) Flow cytometric analyses for BM B220$^{+/-}$ CD138^{high} PCs, and numbers of splenic PCs (Dump^{-} IgD^{-} CD138^{+} Sca-1^{+}) (b, c) Cell numbers for plasma cells in spleen (b) or indicated cell populations in spleen and BM (c) and peritoneal cavity CD19^{+} CD43^{+} B1 B cells (d) in 5-month-old WT;Mb1-Cre and P2rX4$^{f/f}$;Mb1-Cre adults. (For panels (a-c) n=6/group and for panel (d) n=3/group). (e,f) Analysis of B220$^{+/-}$ CD138^{high} BM PCs (e) and all splenic PCs (CD138^{high} Sca-1^{+}) (f) in WT;CD20-TAM-Cre and P2rX4$^{f/f}$; CD20-TAM-Cre adults. (g) Numbers of the indicated T and B cell subsets in the spleen and developing B

cells in BM of the indicated mice. (h) ELISPOT analyses of IgG-secreting BM cells from CD20-TAM-Cre and P2rX4$^{f/f}$;CD20-TAM-Cre mice fed tamoxifen-laced chow for 4 weeks previously. BM cells from tamoxifen-fed mice were cultured for 2 days with or without adding 100μM ATP prior to addition to ELISPOT assay. For panels (e-h) n=6/grp. All bar graphs are means. For panels (a-h) experiments were performed at least thrice. *, p = 0.0022. All p values were derived from two-tailed Mann-Whitney tests, without any adjustment for multiple comparisons.

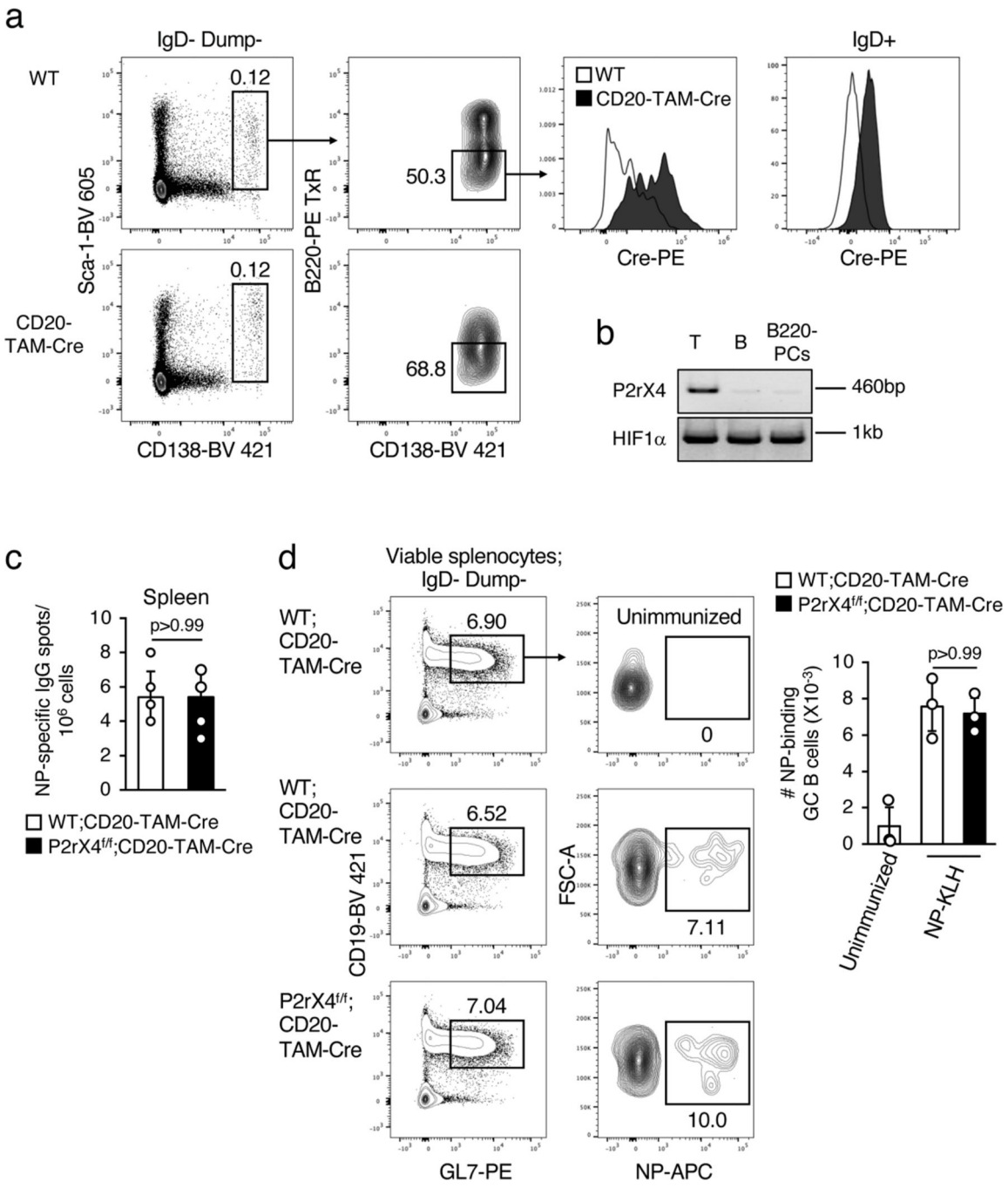

Extended Data Figure 7. Induced B-lineage-restricted P2rX4 mutation in mature BM PCs.

(a) Cre expression in B220^{-} BM LLPCs of CD20-TAM-Cre adults. Data are representative plots of n=3 mice/grp. (b) P2rX4 genomic-PCR for sorted T cells, B cells, and B220^{-} PCs of CD20-TAM-Cre adult mice fed tamoxifen for 1 week (n=3). HIF1α used as a DNA loading control. BM B220^{-} PCs were sorted sequentially twice to ensure purity. For gel source data, see Supplementary Figure 1. (c) NP-specific IgG^{+} PCs in the spleen of the indicated mice. All mice were given tamoxifen-laced chow for 4 weeks beginning at 5 weeks of age, then immunized with NP-KLH/alum and analyzed by ELISPOT 30 days later. Error bars represent the mean (n = 5/grp). (d) NP-specific GC B cells in separate tamoxifen-fed WT;CD20-TAM-Cre and P2rX4$^{f/f}$; CD20-TAM-Cre adults immunized 14 days previously. Graph shows means for hapten-binding GC B cells for 3 mice/group. For a comprehensive illustration of parent gates for evaluating NP-specific GC B cells see extended Figure 3. Experiments in every panel including the PCR data in (b) were performed twice. All p values were derived from two-tailed Mann-Whitney tests for all plots, without any adjustment for multiple comparisons.

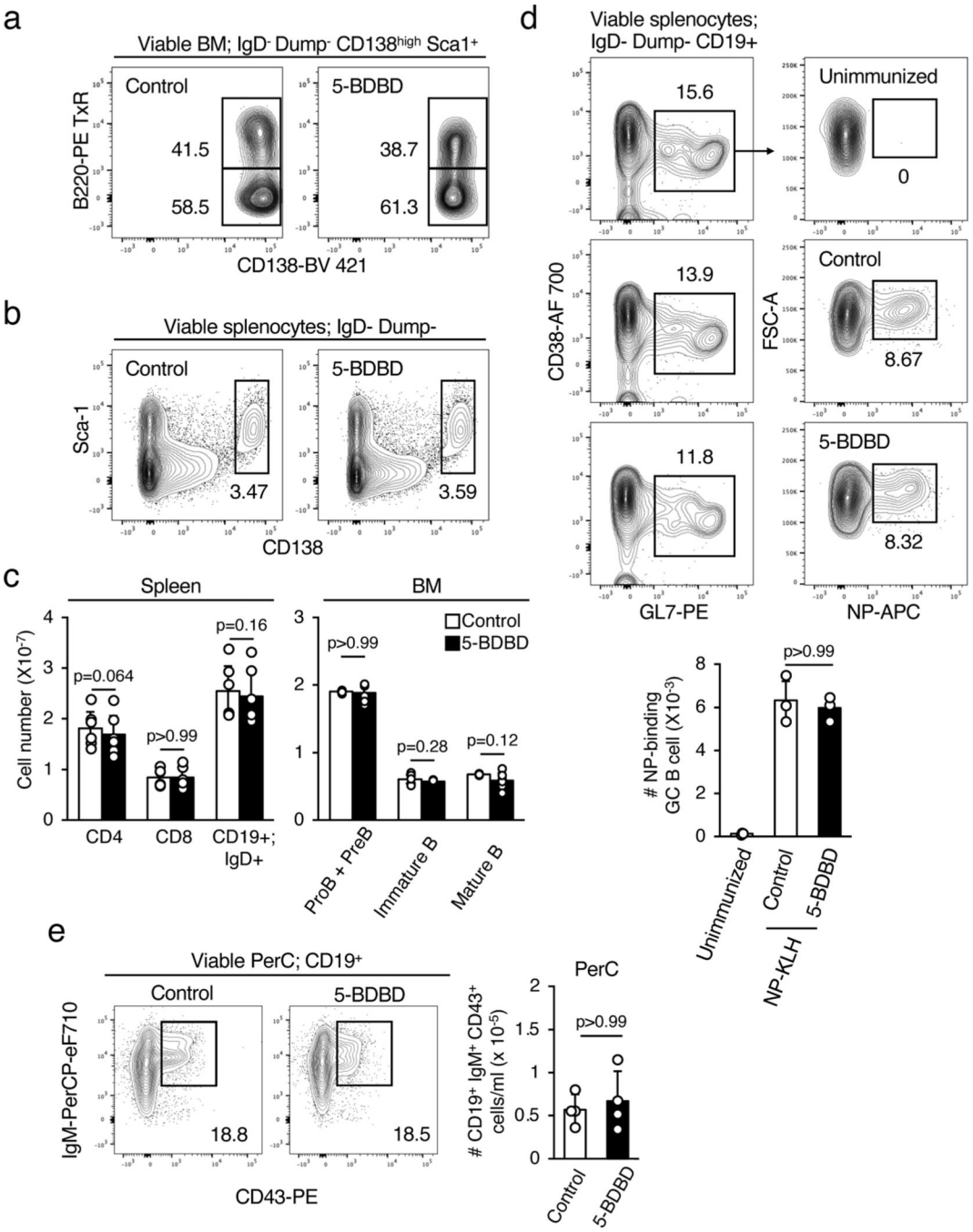

Extended Data Figure 8. Differential impact of P2rX4 inhibition on BM PCs versus naïve and GC B cells.

Flow cytometric analysis of BM and spleen cells from B6 adult females given 5-BDBD (4.25 mg/kg) or DMSO alone as control every 2 days i.v. 4 times. All analyses occurred 8 days after the first dose. (a-c) Shown are steady state B-220$^{+/-}$ BM PCs (a), splenic PCs (b), and naïve splenic T and B cells and BM B-lineage cells (c) from unimmunized mice. For panels (a-c) n=6/grp from one of three experiments. (d) NP-specific GC B cells in separate mice immunized 14 days before with NP-KLH (n=3/grp, representative of two separate experiments). For a comprehensive illustration of parent gates for evaluating NP-specific GC

B cells see extended Figure 3. (e) Numbers and representative flow cytometric analysis of peritoneal cavity CD19^{+} IgM^{+} CD43^{+} B1 B cells in control and 5-BDBD treated C57BL/6 adults. n=4/group. All bar graphs are means. All p values were derived from two-tailed Mann-Whitney tests for all plots, without any adjustment for multiple comparisons.

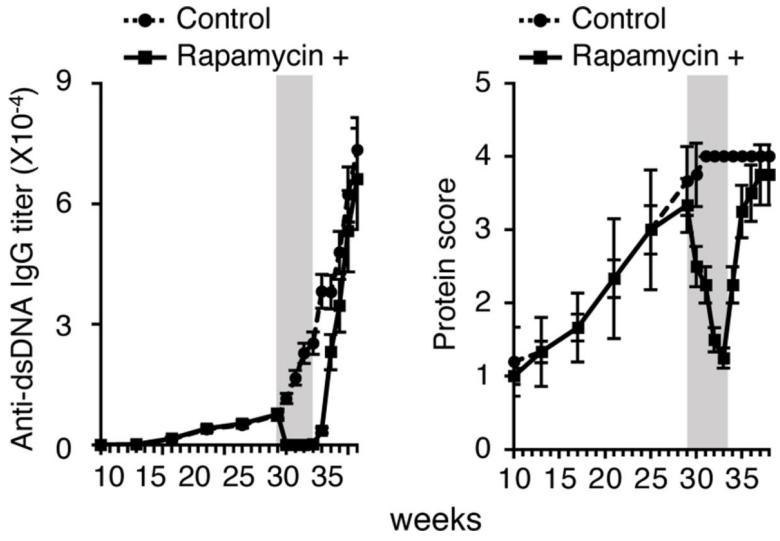

Extended Data Figure 9. Rapid recovery of serum antibody titers and proteinuria following rapamycin.

NZB/W mice were monitored for serum dsDNA-specific IgG titers (a) and urine protein levels (b) over the indicated time frame. Protein scores were graded on a semiquantitative scale: 1, ≥30 mg/dl protein; 2, ≥100 mg/dl; 3, ≥300 mg/dl; and 4, ≥2,000 mg/dl. Twice weekly rapamycin (20 mg/kg) was administered i.v. from 29 to 33 weeks old age. Data represent means and are representative of 2 separate experiments each using 4 mice per group. Treatment windows are shown with gray rectangles.

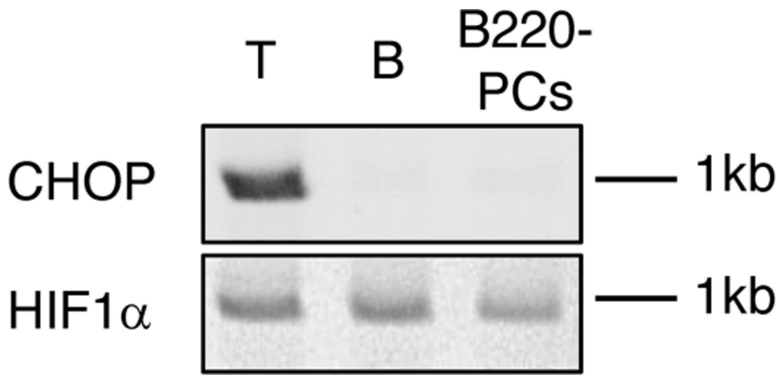

Extended Data Figure 10. Induced CHOP mutation in mature BM PCs.

Genomic DNA was prepared from sorted cells harvested from CHOP$^{f/f}$;CD20-TAM-Cre adults that were fed tamoxifen-laced chow for 4 weeks and evaluated the following day (n=3). Sorted cell populations were mature BM PCs (CD138^{high} Sca-1^{+} B220^{-}) and B (surface IgM^{+}) and T (CD3^{+}) cells that were then subjected to PCR to amplify the CHOP (top) or HIF1a locus. For gel source data, see Supplementary Figure 1.

Supplementary Material

Refer to Web version on PubMed Central for supplementary material.

Acknowledgements

We thank Drs. Michael Cancro, Andre Nussenzweig, Sam John, and Virginia Smith-Shapiro for reviewing this manuscript, Drs. David Hildeman and Ann Marshak-Rothstein for helpful discussions, and Dr. Mark Shlomchik for providing CD20-TAM-Cre mice. We also thank Drs. Maggie Cam and Dina Fonseca for help with statistics, Dr. Hayley Averman for help with histological analysis, and the UPenn Flow Cytometry and Cell Sorting facility.

Funding

This work was supported by National Institutes of Health (NIH) grants R21 AI161931, RO1 AI139123, RO1 AI175185 and an ASPIRE award from the Mark Foundation for Cancer Research to D.A., KAKENHI of Japan grants 16KK0196 and 19K22698 to M.I., NIH grants T32-HL07439 and T32AI007632 to Z.H. and J.L., respectively, an Amyloidosis Foundation Research Grant to Z.H., and the Intramural Research Program of the Center for Cancer Research at the National Cancer Institute (A.B.).

Data availability

Full scans for gels are provided in Supplementary Figure 1. Source data are provided with this paper.

References

1. Radbruch A. et al. Competence and competition: the challenge of becoming a long-lived plasma cell. Nat Rev Immunol 6, 741–750 (2006). [PubMed: 16977339]
2. Jarvis MF & Khakh BS ATP-gated P2X cation-channels. Neuropharmacology 56, 208–215 (2009). [PubMed: 18657557]
3. Borges da Silva H. et al. The purinergic receptor P2RX7 directs metabolic fitness of long-lived memory CD8(+) T cells. Nature 559, 264–268 (2018). [PubMed: 29973721]
4. Burnstock G. P2X ion channel receptors and inflammation. Purinergic Signal 12, 59–67 (2016). [PubMed: 26739702]
5. Ishikawa M. et al. Pannexin 3 functions as an ER Ca(2+) channel, hemichannel, and gap junction to promote osteoblast differentiation. J Cell Biol 193, 1257–1274 (2011). [PubMed: 21690309]
6. Ishikawa M. et al. Pannexin 3 and connexin 43 modulate skeletal development through their distinct functions and expression patterns. J Cell Sci 129, 1018–1030 (2016). [PubMed: 26759176]
7. Wilmore JR, Jones DD & Allman D. Protocol for improved resolution of plasma cell subpopulations by flow cytometry. Eur J Immunol 47, 1386–1388 (2017). [PubMed: 28654161]
8. Jones DD et al. mTOR has distinct functions in generating versus sustaining humoral immunity. J Clin Invest 126, 4250–4261 (2016). [PubMed: 27760048]
9. Cassese G. et al. Plasma cell survival is mediated by synergistic effects of cytokines and adhesion-dependent signals. J Immunol 171, 1684–1690 (2003). [PubMed: 12902466]
10. Burnstock G. Purine and pyrimidine receptors. Cell Mol Life Sci 64, 1471–1483 (2007). [PubMed: 17375261]
11. Hohenegger M. et al. Gsalpha-selective G protein antagonists. Proc Natl Acad Sci U S A 95, 346–351 (1998). [PubMed: 9419378]
12. Jones CA et al. Functional characterization of the P2X(4) receptor orthologues. Br J Pharmacol 129, 388–394 (2000). [PubMed: 10694247]
13. Heng TS, Painter MW & Immunological Genome Project C. The Immunological Genome Project: networks of gene expression in immune cells. Nat Immunol 9, 1091–1094 (2008). [PubMed: 18800157]

14. Tabula Sapiens Consortium. The Tabula Sapiens: A multiple-organ, single-cell transcriptomic atlas of humans. Science 376, eabl4896 (2022).
15. Hobeika E. et al. Testing gene function early in the B cell lineage in mb1-cre mice. Proc Natl Acad Sci U S A 103, 13789–13794 (2006). [PubMed: 16940357]
16. Khalil AM, Cambier JC & Shlomchik MJ B cell receptor signal transduction in the GC is short-circuited by high phosphatase activity. Science 336, 1178–1181 (2012). [PubMed: 22555432]
17. Ahuja A, Anderson SM, Khalil A. & Shlomchik MJ Maintenance of the plasma cell pool is independent of memory B cells. Proc Natl Acad Sci U S A 105, 4802–4807 (2008). [PubMed: 18339801]
18. Yannoutsos N. et al. A cis element in the recombination activating gene locus regulates gene expression by counteracting a distant silencer. Nat Immunol 5, 443–450 (2004). [PubMed: 15021880]
19. Hoyer BF et al. Short-lived plasmablasts and long-lived plasma cells contribute to chronic humoral autoimmunity in NZB/W mice. J Exp Med 199, 1577–1584 (2004). [PubMed: 15173206]
20. Morris SC, Cheek RL, Cohen PL & Eisenberg RA Autoantibodies in chronic graft versus host result from cognate T-B interactions. J Exp Med 171, 503–517 (1990). [PubMed: 2303783]
21. Koshimizu TA et al. Characterization of calcium signaling by purinergic receptor-channels expressed in excitable cells. Mol Pharmacol 58, 936–945 (2000). [PubMed: 11040040]
22. Bettigole SE & Glimcher LH Endoplasmic reticulum stress in immunity. Annu Rev Immunol 33, 107–138 (2015). [PubMed: 25493331]
23. Han J. et al. ER-stress-induced transcriptional regulation increases protein synthesis leading to cell death. Nat Cell Biol 15, 481–490 (2013). [PubMed: 23624402]
24. Puthalakath H. et al. ER stress triggers apoptosis by activating BH3-only protein Bim. Cell 129, 1337–1349 (2007). [PubMed: 17604722]
25. Wilmore JR & Allman D. Here, There, and Anywhere? Arguments for and against the Physical Plasma Cell Survival Niche. J Immunol 199, 839–845 (2017). [PubMed: 28739594]
26. Robinson MJ et al. Intrinsically determined turnover underlies broad heterogeneity in plasma-cell lifespan. Immunity 56, 1596–1612 (2023). [PubMed: 37164016]
27. Benson MJ et al. Cutting edge: the dependence of plasma cells and independence of memory B cells on BAFF and APRIL. J Immunol 180, 3655–3659 (2008). [PubMed: 18322170]
28. O'Connor BP et al. BCMA is essential for the survival of long-lived bone marrow plasma cells. J Exp Med 199, 91–98 (2004). [PubMed: 14707116]
29. Peperzak V. et al. Mcl-1 is essential for the survival of plasma cells. Nat Immunol 14, 290–297 (2013). [PubMed: 23377201]
30. Nikbakht N, Migone TS, Ward CP & Manser T. Cellular competition independent of BAFF/B lymphocyte stimulator results in low frequency of an autoreactive clonotype in mature polyclonal B cell compartments. J Immunol 187, 37–46 (2011). [PubMed: 21632709]
31. Vincent FB, Saulep-Easton D, Figgett WA, Fairfax KA & Mackay F. The BAFF/APRIL system: emerging functions beyond B cell biology and autoimmunity. Cytokine Growth Factor Rev 24, 203–215 (2013). [PubMed: 23684423]
32. Mariathasan S. et al. Cryopyrin activates the inflammasome in response to toxins and ATP. Nature 440, 228–232 (2006). [PubMed: 16407890]
33. Suurvali J, Boudinot P, Kanellopoulos J. & Ruutel Boudinot S. P2X4: A fast and sensitive purinergic receptor. Biomed J 40, 245–256 (2017). [PubMed: 29179879]
34. Fujisaki J. et al. In vivo imaging of Treg cells providing immune privilege to the haematopoietic stem-cell niche. Nature 474, 216–219 (2011). [PubMed: 21654805]
35. Glatman Zaretsky A. et al. T Regulatory Cells Support Plasma Cell Populations in the Bone Marrow. Cell Rep 18, 1906–1916 (2017). [PubMed: 28228257]
36. Zinszner H. et al. CHOP is implicated in programmed cell death in response to impaired function of the endoplasmic reticulum. Genes Dev 12, 982–995 (1998). [PubMed: 9531536]
37. Tellier J. et al. Blimp-1 controls plasma cell function through the regulation of immunoglobulin secretion and the unfolded protein response. Nat Immunol 17, 323–330 (2016). [PubMed: 26779600]

38. Slifka MK, Antia R, Whitmire JK & Ahmed R. Humoral immunity due to long-lived plasma cells. Immunity 8, 363–372 (1998). [PubMed: 9529153]
39. Raje N. et al. Anti-BCMA CAR T-Cell Therapy bb2121 in Relapsed or Refractory Multiple Myeloma. N Engl J Med 380, 1726–1737 (2019). [PubMed: 31042825]
40. Seckinger A. et al. Target Expression, Generation, Preclinical Activity, and Pharmacokinetics of the BCMA-T Cell Bispecific Antibody EM801 for Multiple Myeloma Treatment. Cancer Cell 31, 396–410 (2017). [PubMed: 28262554]
41. Neubert K. et al. The proteasome inhibitor bortezomib depletes plasma cells and protects mice with lupus-like disease from nephritis. Nat Med 14, 748–755 (2008). [PubMed: 18542049]
42. Obeng EA et al. Proteasome inhibitors induce a terminal unfolded protein response in multiple myeloma cells. Blood 107, 4907–4916 (2006). [PubMed: 16507771]
43. Woodle ES, Tremblay S. & Driscoll J. Targeting Plasma Cells with Proteasome Inhibitors: Principles from Primates. J Am Soc Nephrol 28, 1951–1953 (2017). [PubMed: 28592425]
44. Cheng Q. et al. Selective depletion of plasma cells in vivo based on the specificity of their secreted antibodies. Eur J Immunol 50, 284–291 (2020). [PubMed: 31714996]
45. Ralevic V. & Burnstock G. Receptors for purines and pyrimidines. Pharmacol Rev 50, 413–492 (1998). [PubMed: 9755289]
46. Iwamoto T. et al. Pannexin 3 regulates intracellular ATP/cAMP levels and promotes chondrocyte differentiation. J Biol Chem 285, 18948–18958 (2010). [PubMed: 20404334]
47. Wolf FA, Angerer P. & Theis FJ SCANPY: large-scale single-cell gene expression data analysis. Genome Biol 19, 15 (2018). [PubMed: 29409532]
48. Stuart T. et al. Comprehensive Integration of Single-Cell Data. Cell 177, 1888–1902 (2019). [PubMed: 31178118]
49. Lopez R, Regier J, Cole MB, Jordan MI & Yosef N. Deep generative modeling for single-cell transcriptomics. Nat Methods 15, 1053–1058 (2018). [PubMed: 30504886]
50. Traag VA, Waltman L. & van Eck NJ From Louvain to Leiden: guaranteeing well-connected communities. Sci Rep 9, 5233 (2019). [PubMed: 30914743]

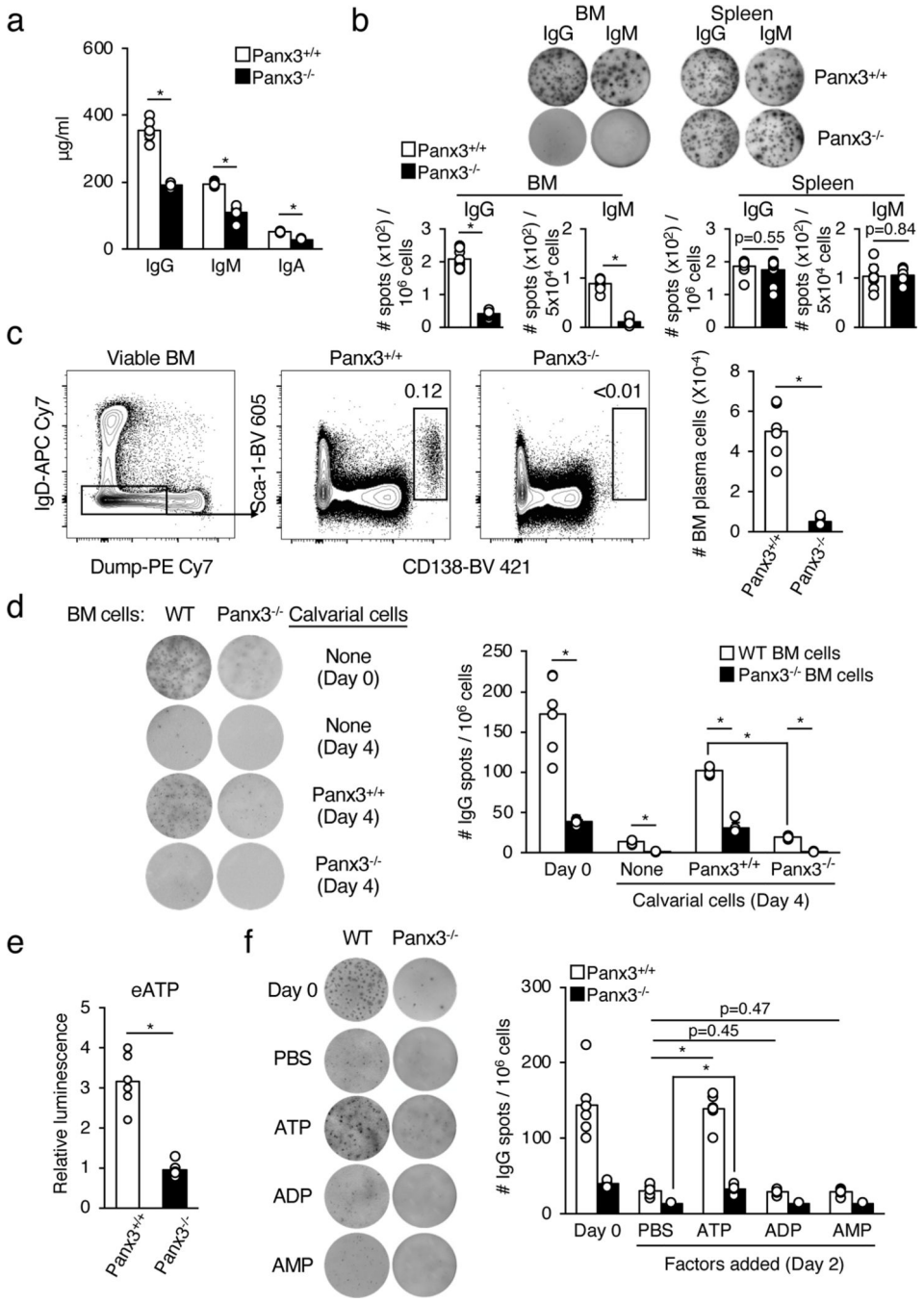

Figure 1. Panx3 mutation ablates BM PCs.

(a) ELISA data for total IgG, IgM and IgA in adult Panx3$^{+/+}$ and Panx3$^{-/-}$ sera. (b) Representative images and quantification of ELISPOT assays for IgG- and IgM-secreting BM and spleen cells from Panx3$^{+/+}$ and Panx3$^{-/-}$ mice. (c) Viable BM PCs from Panx3$^{+/+}$ and Panx3$^{-/-}$ adults. Left-most plot shows representative Dump/IgD gate where the Dump channel is antibodies to CD4, CD8, TER-119 and F4/80. Shown on right are means for BM CD138^{high} Sca-1^{+} cells in the indicated mice. (d) Representative ELISPOT images and numbers of IgG-secreting BM cells from Panx3$^{+/+}$ or Panx3$^{-/-}$ mice on day zero or

after 4 days after culture with osteoblastic calvarial cells from Panx3$^{+/+}$ or Panx3$^{-/-}$ mice. Data shown were combined from 2 experiments. (e) eATP in supernatants from sextuplicate cultures of induced osteoblastic cells from Panx3$^{+/+}$ or Panx3$^{-/-}$ mice. (f) Representative ELISPOT images and numbers of IgG-secreting BM cells on day zero or after addition of 100 μM ATP, ADP or AMP for 48 hours before transfer to ELISPOT wells. For ELISPOT assays 10^6 total cells/well were added except for assays for IgM-secreting cells in (b) where 5×10^4 cells/well were evaluated. n=6/grp for panels (a,c-f); *, p=0.0022. n=9/grp for panel (b); *, p<0.0001. All p values were derived from two-tailed Mann-Whitney tests, without any adjustment for multiple comparisons. All experiments were performed at least thrice except ELISPOT assays in (b) that were performed once for splenic IgG and IgM. All ELISPOT assays plated 1×10^6 cells per well. All bar graphs are means.

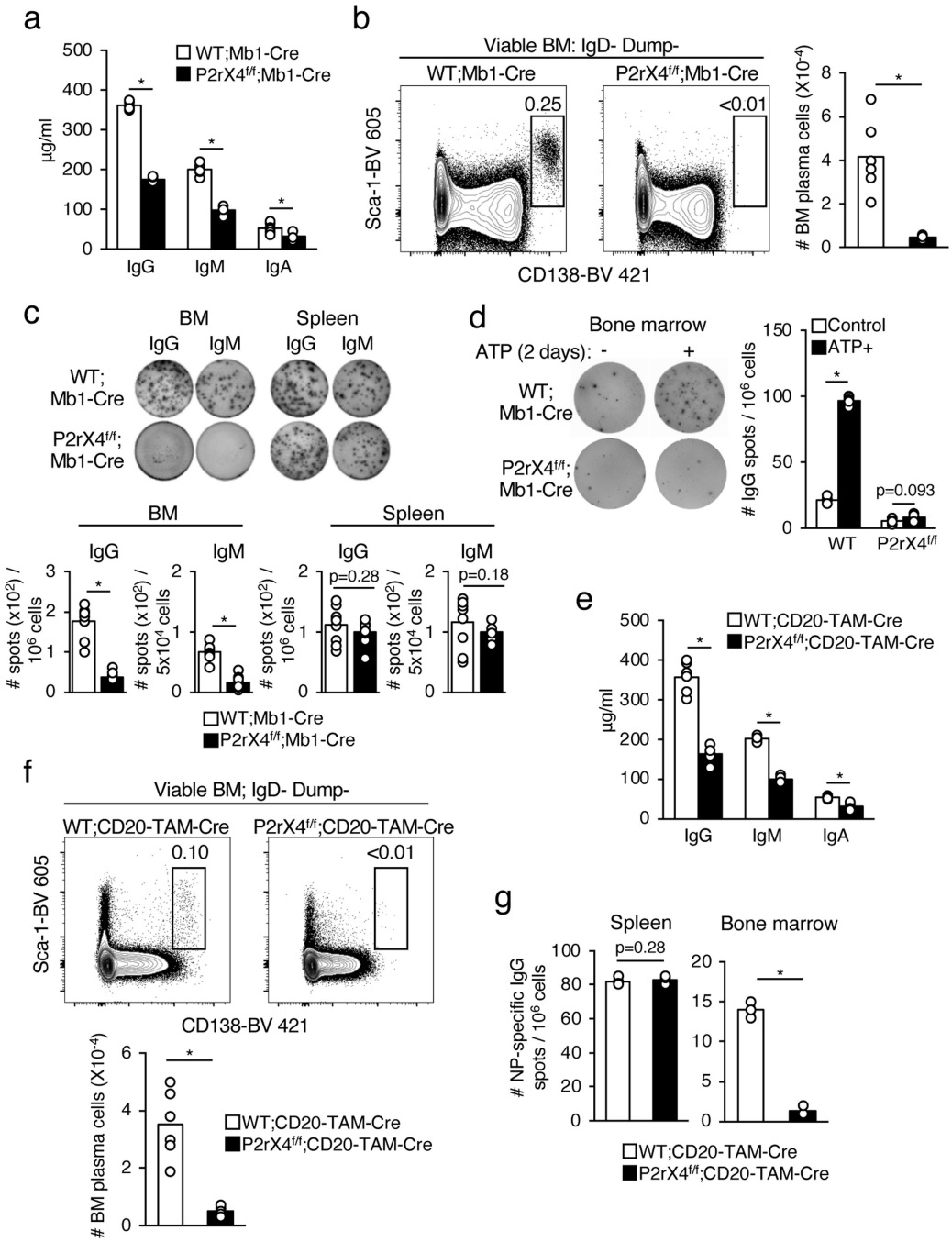

Figure 2. P2rX4 is required for BM PCs.

(a) ELISA data for total IgG, IgM and IgA in sera from WT;Mb1-Cre and P2rX4$^{f/f}$;Mb1-Cre adults. (b) BM PCs in WT;Mb1-Cre and P2rX4$^{f/f}$;Mb1-Cre adults gated on Dump^{-} IgD^{-} cells as shown in Figure 1. (c) Representative images and quantification of ELISPOT wells for IgG-secreting and IgM-secreting BM and spleen cells from WT;Mb1-Cre and P2rX4$^{f/f}$;Mb1-Cre mice. (d) Representative images and quantification of ELISPOT wells for IgG-secreting BM cells from the indicated mice cultured for two days with or without ATP addition before transfer to ELISPOT wells with additional ATP where indicated. (e-g)

WT;CD20-TAM-Cre and P2rX4$^{f/f}$;CD20-TAM-Cre mice were given tamoxifen-laced chow for 4 weeks before direct analysis (e, f) or immunization followed by analysis (g). (e) ELISA data for total IgG, IgM and IgA in sera from WT;CD20-TAM-Cre and P2rX4$^{f/f}$;CD20-TAM-Cre adults immediately after tamoxifen delivery. (f) BM PCs gated as in Figure 1c from WT;CD20-TAM-Cre and P2rX4$^{f/f}$;CD20-TAM-Cre adults fed tamoxifen-laced chow for 4 weeks beginning at 12 weeks of age. (g) WT;CD20-TAM-Cre and P2rX4$^{f/f}$;CD20-TAM-Cre mice were fed tamoxifen for 4 weeks beginning at 5 weeks of age, then immunized with NP-KLH in alum. Shown are ELISPOT analyses for NP-specific PCs in spleen and BM on day 7 and 30 post-immunization, respectively. For ELISPOT assays 10^6 total cells/well were added except for assays for IgM-secreting cells in (c) where 5×10^4 cells/well were evaluated. n=6/grp for panels (a,b,d-g); *, p=0.0022. n=9/grp for panel (c); *, p<0.0001. All p values were derived from two-tailed Mann-Whitney tests, without any adjustment for multiple comparisons. The experiments in panels (a, b, d-f) were performed at least thrice. The experiments in panel (c) were performed at least twice and the experiment in panel (g) was performed twice. All bar graphs are means.

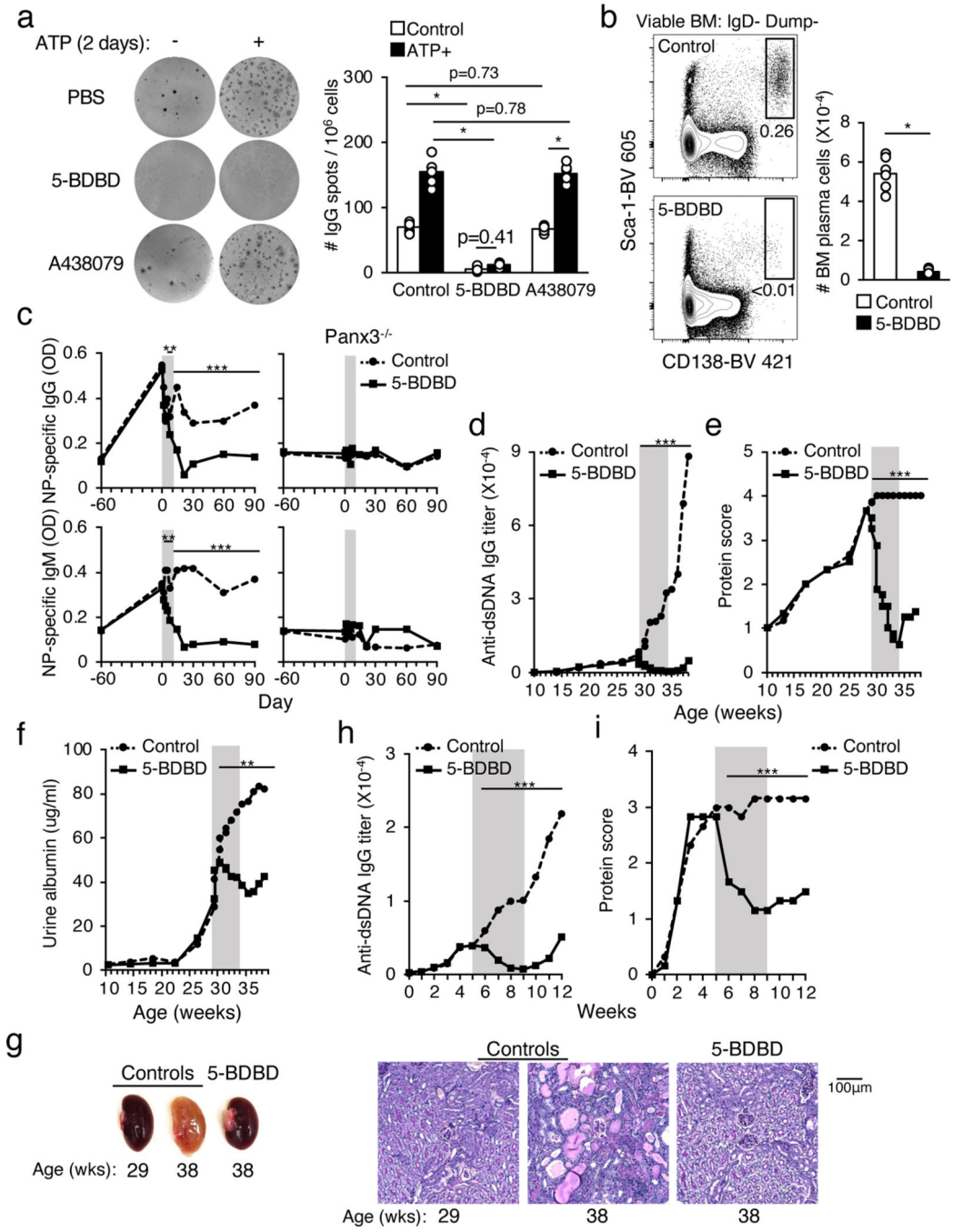

Figure 3. P2rX4 inhibition causes loss of serum antibodies by depleting BM PCs.

(a) ELISPOT analyses for total IgG-secreting cells among B6 BM cells (10^6 cells/well) first cultured with or without 100 μM ATP and with or without 50 μM 5-BDBD or 50 μM A438079 versus DMSO alone for 2 days. (b) B6 adult females were given four injections of 5-BDBD (4.25 mg/kg) or DMSO i.v. (n=6/grp.) every 2 days and then analyzed on day 8. $Dump^-$ IgD^- gate shown in Figure 1. (c) 5-BDBD depletes pre-established serum antibodies. B6 and $Panx3^{-/-}$ females were immunized with NP-KLH/alum. Sixty days later ("day 0") mice were given DMSO (dotted line) or 5-BDBD (solid line) five times over 10

days (n=3/grp). Shown are optical density (OD) values for NP-binding serum IgG and IgM at each time point.(d-g) NZB/W females were given DMSO (dotted line) or 5-BDBD (solid line) at 29–33 weeks of age (gray rectangles). Shown are anti-dsDNA antibody titers (d), overall proteinuria (e) (see Methods for scoring), urine albumin (f), kidney pigmentation and histological images revealed with PAS staining (g). (d, e) n=6/grp; (f, g) n=3. (h, i) B6 adults previously given B6.H2-Ab1^{bm12} splenocytes (“day 0”) were given 5-BDBD (solid line) or DMSO (dotted line) (n=3/grp.) at 5–9 weeks post-cell transfer (gray rectangles) and monitored for dsDNA-specific serum IgG (h) and proteinuria (i). Means are shown for all graphs. For panels (a,b), *, $p = 0.0022$, with p values derived from two-tailed Mann-Whitney tests, without any adjustment for multiple comparisons. For (panels c-f, h, i) *, $p < 0.05$, **, $p < 0.01$, ***, $p < 0.001$., derived from a repeated measures ANOVA (see Methods). The experiments in panels (a-b) were performed at least thrice, and the experiments in panels (c-e) and (g-i) were performed twice.

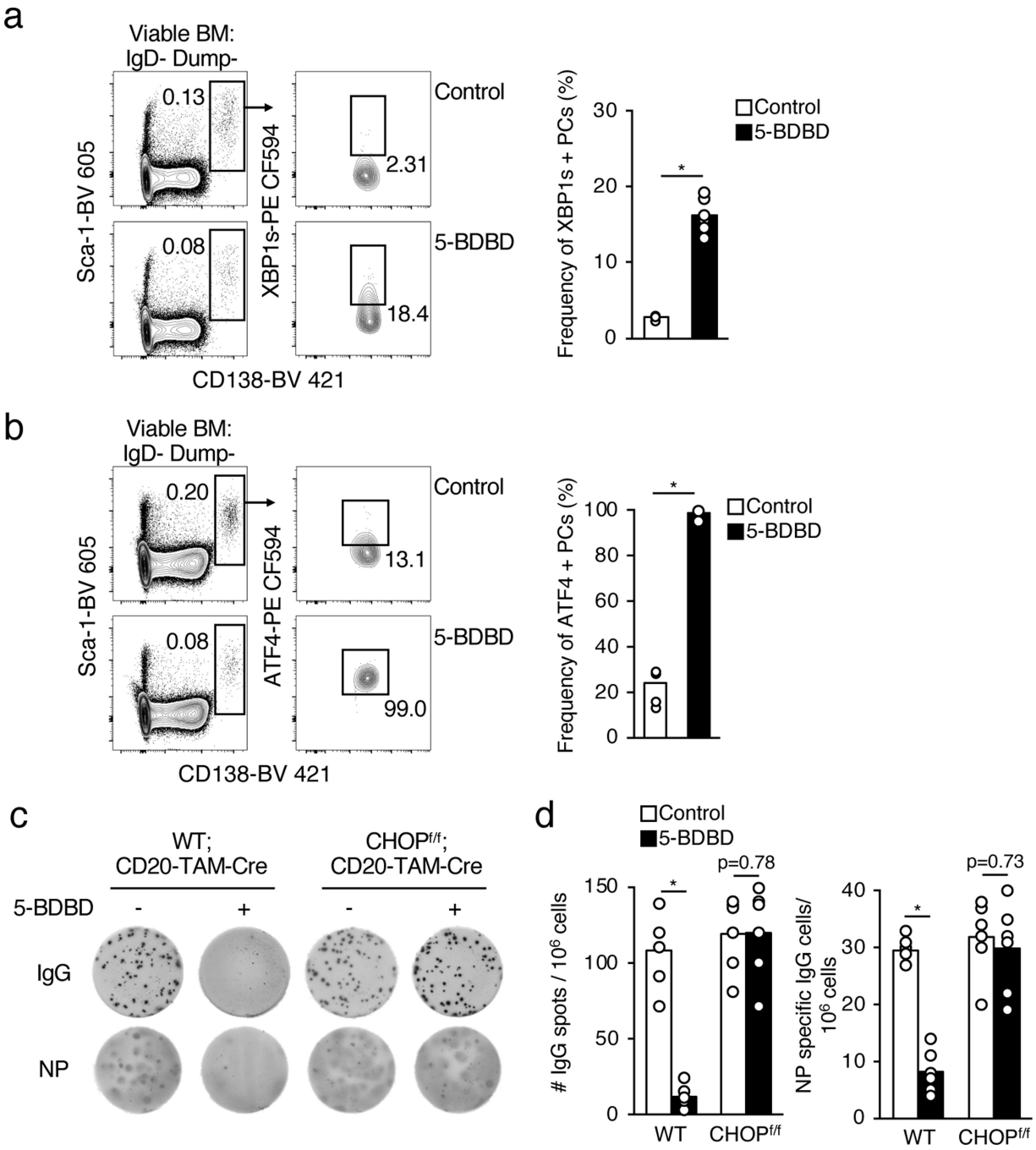

Figure 4. P2rX4 inhibits ER-affiliated apoptosis in BM PCs.

Intracellular XBP1s (a) and ATF4 (b) expression for BM PCs 24 hours after treating mice once with 5-BDBD or DMSO alone (control) (n=6/grp.). (c,d) WT;CD20-TAM-Cre and CHOP$^{f/f}$;CD20-TAM-Cre adults were fed tamoxifen-laced chow for 4 weeks before immunization with NP-KLH/alum. 4 weeks post-immunization cohorts were given 5-BDBD (4.25 mg/kg) or DMSO thrice i.v. for 7 days before analysis (n=6/grp.). Representative images (c) and quantification (d) of ELISPOT analyses of 10^6 total cells/well for total (left) and NP-specific BM PCs (right) in indicated mice. All bar graphs are means. Data in (d) are

pooled from two experiments with a total of 6/grp. For panels (a,b,d), *, p = 0.0022, with p values derived from two-tailed Mann-Whitney tests without any adjustment for multiple comparisons. All experiments were performed at least twice.